IOPscience iopscience.iop.org

Home Search Collections Journals About Contact us My IOPscience

Structural, electrical, magnetic and microstructural behavior of the $La_{0.7}Sr_{0.3-x}Hg_xMnO_3$ ($0 \leq x \leq 0.3$) system

This article has been downloaded from IOPscience. Please scroll down to see the full text article.

2008 J. Phys.: Condens. Matter 20 395218

(http://iopscience.iop.org/0953-8984/20/39/395218)

View the table of contents for this issue, or go to the journal homepage for more

Download details:
IP Address: 129.252.86.83
The article was downloaded on 29/05/2010 at 15:13

Please note that terms and conditions apply.

J. Phys.: Condens. Matter **20** (2008) 395218 (9pp) doi:10.1088/0953-8984/20/39/395218

Structural, electrical, magnetic and microstructural behavior of the $La_{0.7}Sr_{0.3-x}Hg_xMnO_3$ ($0 \leqslant x \leqslant 0.3$) system

Vilas Shelke[1], A Das[2], Indu Dhiman[2], Rashmi Yadav[1], Subhash Khatarkar[1], Avneesh Anshul[1] and R K Singh[1]

[1] Department of Physics, Barkatullah University, Bhopal 462 026, India
[2] Solid State Physics Division, Bhabha Atomic Research Center, Mumbai 400 085, India

E-mail: drshelke@gmail.com

Received 19 May 2008, in final form 16 July 2008
Published 1 September 2008
Online at stacks.iop.org/JPhysCM/20/395218

Abstract

We report a detailed investigation on the polycrystalline samples of the colossal magnetoresistance system $La_{0.7}Sr_{0.3-x}Hg_xMnO_3$ ($0 \leqslant x \leqslant 0.3$). The emphasis is put on identifying the role of Hg in the perovskite matrix. We have used the neutron diffraction technique for structural analysis. The issues pertaining to composition-dependent variations in parameters like average ionic radii, tolerance factor, variance, bond length, bond angle, lattice parameters and cationic vacancies have been addressed. The low temperature resistivity measurement and subsequent curve fitting are used to explore the contributions from various disorders and interactions. The samples with $x = 0.3$ composition showed distinct electrical behavior and magnetoresistance up to 46% around $T = 198$ K. The low temperature neutron diffraction data revealed ferromagnetic character of the samples. All the samples displayed similar microstructures. The variations in the electrical and magnetic properties are attributed to origination from cationic disorders.

1. Introduction

The electrical or magnetic transitions under the influence of external stimuli have attracted researchers for several years. Traditionally, such stimuli are applied by changing thermodynamic variables, like temperature, pressure, magnetic field, etc. The highly celebrated example is the metal–insulator transition exhibited by several systems [1]. Ever since the inception of the concept of Mott insulators, several pioneers investigated the criterion for minimum metallic conductivity and a suitable mechanism from time to time [2–4]. The recent developments in the study of perovskite oxides, particularly lanthanum manganites, revived this topic [5, 6]. The lanthanum manganites exhibit large numbers of electrical, magnetic and structural phases embedded together in composition and temperature scale [7]. An amazing fact is the coexistence of the complementary phases in the form of subatomic scale inhomogeneities [8, 9]. The display of mutually exclusive phases, like charge ordered insulators and ferromagnetic metals by adjoining grains of the same sample, is highly exotic. Nevertheless, they also carry tremendous application potentials due to their spintronics ability [10]. A flurry of activity in terms of spin polarized, spin injection and spin tunneling devices has already been initiated [11].

The competition between localization and delocalization of electrons governs the variant physical properties of the manganites. The key role in proper tuning of the desired property is played by the crystal chemistry. The highly susceptible nature of the perovskites in terms of crystal and electronic structures is widely documented [5, 6]. It provides a handy tool to control two fundamental parameters, namely bandwidth and band filling, to manipulate the physical properties [3]. The bandwidth corresponds to the electron correlation strength and it can be altered by application of external mechanical pressure or generation of internal chemical

 © 2008 IOP Publishing Ltd Printed in the UK

pressure through lattice distortion within the tolerance limit. The tolerance factor is directly related to the ionic radii through the relation $t = (\langle r_A \rangle + r_O)/\sqrt{2}(r_{Mn} + r_O)$ and it determines the lattice parameters, Mn–O bond length and Mn–O–Mn bond angle. The distorted perovskite structure is sustainable over a wide range $0.89 \leqslant t \leqslant 1.02$ [7]. The deviation of t from the unit value can reduce the one-electron bandwidth by 30–40% [3]. Therefore, varieties of iso-valent rare earth compositions are reported [3, 5]. Alternatively, the band filling relies on the substitution of alio-valent ions, which creates excess charge carriers through hole or electron doping. The substitutions at the Mn site are comparatively more destructive. The oxygen non-stoichiometry also plays a critical role. It can moderate the electronic structure in the local arena through creation of vacancies and interstitials.

The divalent elements like Sr, Ca, Ba and Pb are mostly preferred for the substitution at the 'A' site. These elements form a complete range of solid solutions and produce well-known magnetic phase diagrams [6]. The substitution studies on other elements like Ag [12–16], Bi [17], Te [18] and Cd [19] are also reported. However, scant attention has been paid towards the substitution of divalent Hg in lanthanum manganites [20, 21]. The Hg-based systems and its substitution in other systems are extensively studied in the context of superconducting cuprates. The ionic radius of Hg^{2+} with eightfold coordination is 1.14, which is well within the tolerance limit of the perovskite structure. Therefore, it is a potential element to impart crystal and electronic structural modifications. The intentional disorders arising from inherent chemical randomness or impurity doping cause major modifications in the magneto-electronic properties [6]. We have recently reported the synthesis of the $La_{0.7}Sr_{0.3-x}Hg_xMnO_3$ ($0 \leqslant x \leqslant 0.2$) system [21]. We found that HgO addition improves the temperature range over which a significant magnetoresistance can be observed. Such wide range colossal magnetoresistance is required to enhance the applicability of this phenomenon for meaningful device fabrications. In juxtaposition, it is important to address the specific role of 'Hg' ions in the basic matrix. It is necessary to explore the nature of such substitution and the underlying transport mechanism. We investigated the structural implications through the powder neutron diffraction technique. The vital parameters identified in the present case are the tolerance factor, bond angle, cationic vacancies and associated disorders. We also elaborate the charge transport mechanism on the basis of low temperature resistivity data and the curve fitting process. The magnetoresistance up to 46% and unusual magnetization with broad transition is observed in some samples. The similarity in grain morphology at the microscopic level points towards the intrinsic character of the charge carrier scatterings.

2. Synthesis and characterization

We have synthesized several polycrystalline samples with nominal compositions $La_{0.7}Sr_{0.3-x}Hg_xMnO_3$ ($0 \leqslant x \leqslant 0.3$) by the standard solid state reaction method using La_2O_3 (Aldrich, 99.99%), $SrCO_3$ (Aldrich, 99.995%), MnO_2 (Aldrich, 99.99%) and HgO (Aldrich, 99.9%) compounds. The homogeneous mix was calcined in air at 950 °C for 24 h with intermediate grinding. The circular pellets of 12 mm diameter were sintered at 1100 °C in air for 30 h followed by furnace cooling.

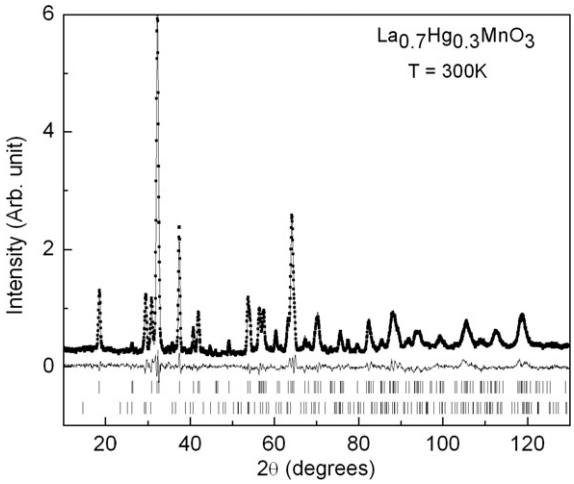

Figure 1. Neutron diffraction pattern of the $La_{0.7}Hg_{0.3}MnO_3$ sample at 300 K. The observed data and the fit to it are indicated as symbols and a solid line, respectively. The tick marks show the allowed reflections (upper $La_{0.7}Hg_{0.3}MnO_3$, lower Mn_3O_4) and the lower solid line is the difference plot.

Neutron diffraction patterns were recorded at several temperatures between 15 and 300 K on the PSD-based multi-detector powder diffractometer ($\lambda = 1.249$ Å) at Dhruva, BARC. Crystal and magnetic structure refinement was carried out using the FULLPROF program [22]. The zero-field resistance as a function of temperature was measured by the standard four-probe method in the temperature range 20 K $\leqslant T \leqslant$ 300 K. A constant current of 10 mA was passed through the samples. We used a superconducting magnet (Oxford Spectromag 2000) in persistent mode for the resistivity measurements in high magnetic field. The magnetoresistance was defined as $MR = [(R_0 - R_H)/R_0] \times 100\%$, where R_0 and R_H are resistance without and with a magnetic field, respectively. The magnetization as a function of temperature was measured by the vibrating sample magnetometer with a field of 30 Oe in the temperature range 80 K $\leqslant T \leqslant$ 300 K. The microstructure of the bulk samples was studied by a scanning electron microscopy technique.

3. Results and discussion

3.1. Structural investigations

All the four samples in the series $La_{0.7}Sr_{0.3-x}Hg_xMnO_3$ ($0 \leqslant x \leqslant 0.3$) are isostructural. Profile refinements of the neutron diffraction data at 300 K show that all the compositions crystallize in the rhombohedral structure. They have been analyzed in the trigonal space group ($R\bar{3}c$) hexagonal setting ($z = 6$). Figure 1 shows the neutron diffraction pattern for $x = 0.3$ at 300 K. This is a typical diffraction pattern for the whole series. The La/Sr/Hg atoms occupy position 6a[0, 0, 1/4], Mn

Table 1. The structural data obtained from the refinement of neutron diffraction patterns at 300 K and calculated values of tolerance factor, variance, average ionic radii for twelvefold coordination for the samples with nominal compositions $La_{0.7}Sr_{0.3-x}Hg_xMnO_3$ ($0 \leqslant x \leqslant 0.3$). The space group $R\bar{3}c$ was used. The atomic sites are La/Sr/Hg 6a[0, 0, 1/4]; Mn 6b[0, 0, 0]; O 18e[x, 0, 1/4]. Numbers in parentheses are statistical errors in the least significant digit.

Parameters	$x = 0.0$	$x = 0.1$	$x = 0.2$	$x = 0.3$
$\langle r_A \rangle$ (Å)	1.3840	1.3665	1.3490	1.331
t	0.9809	0.9747	0.9685	0.9623
σ^2(Å^2)	0.0013	0.0021	0.0023	0.0032
a (Å)	5.5059(5)	5.5186(6)	5.5325(9)	5.5390(7)
c (Å)	13.3629(3)	13.3698(2)	13.3957(2)	13.4042(2)
V (Å^3)	350.83(1)	352.62(2)	355.08(7)	356.14(6)
La/Sr/Hg B (Å^2)	0.9(1)	0.9(1)	1.3(1)	1.3(1)
Mn B (Å^2)	0.5(1)	0.5(1)	0.5(1)	0.5(1)
O x	0.4575(5)	0.4535(5)	0.4505(4)	0.4473(5)
B (Å^2)	1.3(1)	1.3(1)	1.6(1)	1.6(1)
La/Sr/Hg–O (Å)	2.5192(22)	2.5030(30)	2.4928(25)	2.4780(28)
Mn–O (Å)	1.9547(12)	1.9608(15)	1.9676(16)	1.9721(14)
Mn–O–Mn (deg)	175.22(20)	174.77(30)	174.43(40)	174.07(25)
M (μ_B)	1.1(1)	1.1(1)	0.3(1)	0
Mn_3O_4 (%)	0	1.7(0.5)	4(1)	5(1)
Refined stoichiometry	$La_{0.7}Sr_{0.3}MnO_3$	$La_{0.7}Sr_{0.19(1)}Hg_{0.09(1)}MnO_3$	$La_{0.7}Sr_{0.09(1)}Hg_{0.18(2)}MnO_3$	$La_{0.7}Hg_{0.25(2)}MnO_3$
R_{exp}	5.52	7.4	5.01	4.7
R_{wp}	12.7	20.2	9.36	8.24
R_p	9.8	13.2	7.4	6.5
R_B	12.8	12.1	8	9.2

at 6b[0, 0, 1/2] and O at 18e[x, 0, 1/4]. Positional parameters of oxygen, isotropic temperature factors, cell parameters and occupancies were varied. To refine occupancies it was assumed that only the Sr and Hg concentration would deviate from its starting stoichiometry, because of the high volatility of Hg. Therefore, all other occupancies were held fixed. Refined composition show deficiencies in the 'A' site. Our data revealed the presence of the Mn_3O_4 phase in the samples $x \neq 0$. The percentage of the Mn_3O_4 phase increases for higher values of x, although it is less than 5%. The refined stoichiometry indicates the substitution of 'Hg' at the 'La' site with a value lower than the nominal value. The lower stoichiometry can result from the partial escape of the Hg due to HgO decomposition at elevated temperatures. A systematic variation of the structural parameters with x can further substantiate the Hg incorporation in the matrix. The magnetic transition temperatures of all the samples, except $x = 0.3$, are above 300 K. Therefore the refinements included the magnetic phase in addition to the chemical structure. The refined parameters are included in table 1.

The widely referred-to parameter, in substitution studies, is the Goldsmith tolerance factor (t). It relies on the custom concept of distance as an algebraic sum of ionic radii, resulting in $t = (r_A + r_O)/[\sqrt{2}(r_B + r_O)]$. When an A-site ion is partially substituted by an alio-valent ion, there is a proportional change in the average radii of the A site as well as in the valence of the B site. Then, $t = (\langle r_A \rangle + r_O)/[\sqrt{2}(\langle r_B \rangle + r_O)]$, where $\langle r_A \rangle$ and $\langle r_B \rangle$ are composition averaged ionic radii of 'A' and 'B' sites, respectively, and r_O is the ionic radius of oxygen. This approach has a drawback as the ionic radii itself depends on the coordination environment, oxidation, spin state, etc. At low values of $\langle r_A \rangle$, the MnO_6 octahedra bends around a small 'A' ion in such a way that the A–O distance is less for 9 oxygen atoms and greater for the remaining 3, thereby making effectively ninefold coordination. At larger values of $\langle r_A \rangle$, twelvefold coordination is acquired [23]. Thus, the coordination number depends on ionic radii and vice versa. The variation in reported 't' values for the same composition is largely due to the selection of ionic radii with different coordination numbers from the Shannon tables [24]. Sometimes, the necessary 12-coordinate 'A' site radii and 6-coordinate 'B' site radii are determined through extrapolation. Alternatively, the tolerance factor is written in terms of the bond lengths [25]. The bond lengths A–O and B–O are used assuming 12 equidistance A–O bonds and 6 equidistance B–O bonds. In terms of bond lengths in a perovskite structure, the tolerance factor $t = d_{A-O}/(\sqrt{2}d_{B-O})$, where d_{A-O} and d_{B-O} are the lengths of the A–O and B–O bonds, respectively. In addition, the substitution may introduce local perturbation in terms of cationic disorder or variance [26] given by $\sigma^2 = \langle r_A^2 \rangle - \langle r_A \rangle^2 = \sum x_i r_i^2 - \langle r_A \rangle^2$. Determination of variance depends on the selection of the values of ionic radii.

We have given the comprehensive structural data of our samples in table 1. The average ionic radii, tolerance factor and variance are calculated using ionic radii for twelvefold coordination of 'A' ions, sixfold coordination of Mn ions and twofold coordination of oxygen anions. The relevant neutron diffraction patterns for the samples with compositions $La_{0.7}Sr_{0.3-x}Hg_xMnO_3$ ($0 \leqslant x \leqslant 0.3$) obtained at 300 K are shown in figure 2. The neutron diffraction patterns are refined

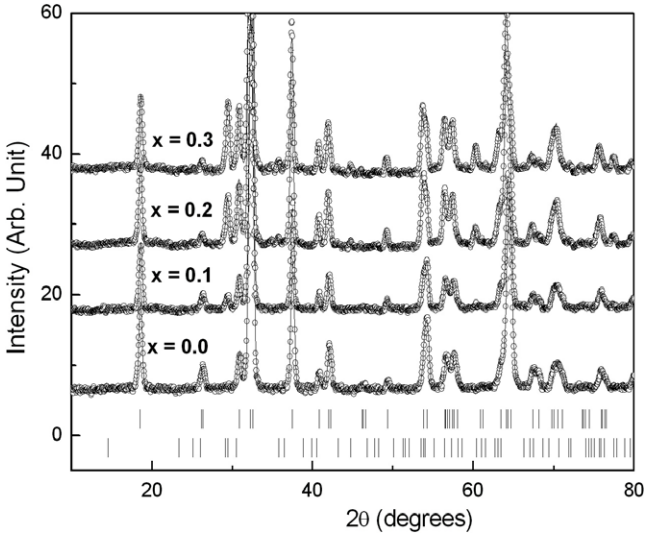

Figure 2. The sections of neutron diffraction patterns for the samples with nominal compositions $La_{0.7}Sr_{0.3-x}Hg_xMnO_3$ ($0 \leqslant x \leqslant 0.3$) recorded at 300 K. The solid line corresponds to the fit to the data. The tick marks show the allowed reflections (upper $La_{0.7}Sr_{0.3-x}Hg_xMnO_3$, lower Mn_3O_4).

in the rhombohedral ($R\bar{3}c$) space group. The rhombohedral structure has been reported for $0.96 \leqslant t \leqslant 1$, where the tolerance factor is for twelvefold coordinated ionic radii [7]. In the present case, the corresponding t values are above 0.9623. Recently, XANES and EXAFS studies by Dezanneau *et al* have demonstrated that La occupancy less than 0.9 results in segregation of parasitic phases, like Mn_3O_4 [27]. The departure from its ideal value of $t = 1$ indicates the presence of distortion. The rhombohedral distortion may be viewed as a rotation of the octahedra around the threefold axis by an angle ω from the ideal perovskite structure. This rotation describes the buckling of the MnO_6 octahedra caused by ionic radii mismatch between A and B cations. The angle of rotation ω may be calculated from the oxygen position using $\omega = \arctan(\sqrt{3} - x\sqrt{12})$ [28]. The values obtained are 8.3, 9.15, 9.73 and 10.34 degrees for $x = 0$, 0.1, 0.2 and 0.3, respectively. It indicates increasing tilting of the octahedra with Hg substitution. An increase in variance, σ^2 from 1.3×10^{-3} to 3.2×10^{-3} is observed on increasing Hg concentration. Though this affects substantially the structural, electrical and magnetic properties, it is possibly too weak a disorder to result in an increase of diffuse scattering. This is evident from the diffraction patterns in figure 2, where we do not observe any change in the width of Bragg peaks or change in the background as a function of composition. To study the role of disorder in this kind of system pair distribution function analysis of the neutron diffraction pattern is a more reliable technique rather than the average picture obtained from the Rietveld refinement as done in the present case.

It is clear from table 1 that there is a wide variation in the values of t, σ^2 and $\langle r_A \rangle$ as a function of composition. Since Hg^{2+} is a smaller ion, a gradual decrease in the values of t and $\langle r_A \rangle$ with increasing x is expected. The variation in the values of the variance is because of ionic radii mismatch. The reported values of the variance are in the range 4.53×10^{-4} for $Pr_{0.7}Ca_{0.3}MnO_3$ to 1.16×10^{-1} for $La_{0.7}Ba_{0.3}MnO_3$ [23]. Our neutron diffraction data revealed composition-dependent variations of bond lengths and bond angles. The values are similar to the data reported earlier for the different compositions of similar average ionic radii [23, 29]. The A–O bond length decreases with increasing x as a result of lowering average ionic radii of the 'A' site. A slight increase in Mn–O bond length is also observed. The structural evolution depends on the degree of distortion (tilting of octahedra) and the axis of rotation. The consequences of the tilting are reflected by the change in bond length and bond angle [30]. At $x = 0$, the value of Mn–O–Mn bond angles (Φ) is 175.22°, just 4.78° lower than the ideal value of 180°. The angle decreases up to the value 174.07°, which means the bending increases for $x = 0.3$. The evolution of lattice parameters with composition indicates a gradual increase in the parameters a and c. The unit cell volume exhibits a more significant change. The increase in the unit cell volume is due to increasing distortion of the MnO_6 octahedra and augments the Mn–O bond lengths [19, 26]. The structural parameters like bond angles and lengths for $x = 0$ can be compared with the reported values of this compound. In this case, the cell parameters and the bond lengths obtained at 300 K are in good agreement with the published results on the same compound [31].

3.2. Electrical and magnetic behavior

The basic system under investigation with $x = 0$ is $La_{0.7}Sr_{0.3}MnO_3$. This is a band-filled system with larger bandwidth of the e_g electron due to the larger size of the Sr^{2+} ions and, as such, it exhibits metallic character well above room temperature [6]. Ideally, replacement of divalent Sr by the iso-valent Hg is not expected to introduce any additional band filling. However, the change in ionic size can alter the e_g bandwidth. In addition, the atomic scale disorders as revealed by the neutron diffraction data can influence the band filling. The variation of electrical resistivity with temperature for $La_{0.7}Sr_{0.3-x}Hg_xMnO_3$ ($0 \leqslant x \leqslant 0.2$) samples is shown in figure 3. A preliminary report on the zero and high field resistance measurement of these samples has been published elsewhere [21]. These samples showed typical metallic behavior within the temperature range 20 K $\leqslant T \leqslant$ 300 K. In the low temperature region the resistivity values are within the range 2.5–12.5 mΩ cm for these samples. It is of the order of Mott's criterion for maximum metallic resistivity of oxides [1]. The manganites are not very particular in following Mott's criterion, as the residual resistivity is reported to vary from 10^{-4} Ω cm for LaSrMnO to 10^4 Ω cm for the NdSrMnO system [32]. These variations are on account of variant 3d bands and perturbations in the periodic potentials by several disorders in these oxides. It is also clear from figure 3 that for higher values of x, i.e. lower values of $\langle r_A \rangle$, the magnitude of resistivity is higher at all temperatures. Garcia-Munoz *et al* have reported that the smaller values of $\langle r_A \rangle$ correspond to small tolerance factors or Mn–O–Mn bond angles (Φ) [33]. The lower value of Φ causes weakening of the hybridization of Mn e_g and O 2p orbitals. We fitted resistivity data of our

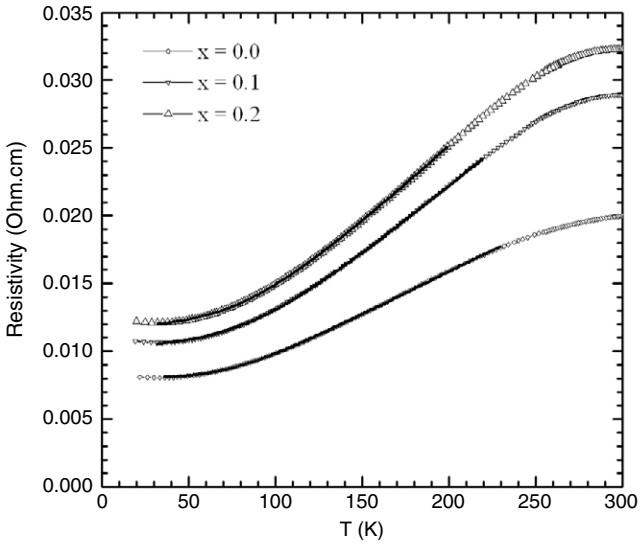

Figure 3. The variation of zero field electrical resistivity with temperature for the samples with composition $La_{0.7}Sr_{0.3-x}Hg_xMnO_3$ ($x = 0.0, 0.1, 0.2$). Solid lines are curves fitted to equation (1).

samples in the metallic region to the equation of the form [34]–

$$\rho(T) = \rho_0 + \rho_1 \frac{T^5}{\theta_D^6} \int_0^{\theta_D/T} \frac{x^5\,dx}{(1-e^x)(1-e^{-x})} + \rho_2 T^{3/2}. \quad (1)$$

In this equation, the first term ρ_0 is the residual resistivity due to static disorders; the second term is the Bloch–Gruneisen integral for electron–phonon interaction and the third term is associated with electron-magnetic scattering. The coefficients $\rho_1\rho_2$, residual resistivity ρ_0 and Θ_D, the Debye temperature, are the fitting parameters. The residual resistivity, ρ_0 is found to increase with x. This is attributed to an increase in disorder due to substitution of Hg and Mn_3O_4 impurities. The temperature dependence of resistivity is influenced by a shallow minimum below 40 K and the metal–insulator transition above 240 K. The true metallic behavior described by equation (1) holds in the range between 40 and 240 K in these samples. Therefore, the resistivity data has been fitted to equation (1) in the range between 40 and 240 K. The fitted curves are indicated in figure 3 by solid lines and the fitting parameters for all the samples are given in table 2. The curve fitting justifies that in the metallic regime the carrier transport is influenced by the temperature-independent disorders as well as the electron–phonon and electron–magnon scatterings. The magnetic scattering term is relatively small compared to the electron–phonon term. The magnetic term in resistivity of itinerant ferromagnets is found to be proportional to T^2 and $T^{3/2}$ for single-particle excitations and collective particle excitations, respectively [35]. We find that the $T^{3/2}$ term in addition to the phonon term describes our data better in the metallic regime. This equation describes the transport behavior better than the polynomial equations given in the literature [35–40] because we are able to attribute each term to magnetic and nonmagnetic scattering without ambiguity. In the limit $T \ll \Theta_D$, the phonon term is proportional to T^5. The general dependence of resistivity on temperature in the metallic

Table 2. The curve fitting parameters for the resistivity as a function of temperature according to equation (1) for the samples with nominal compositions $La_{0.7}Sr_{0.3-x}Hg_xMnO_3$ ($0 \leqslant x \leqslant 0.2$).

Parameters	$x = 0.0$	$x = 0.1$	$x = 0.2$
ρ_0 (Ω cm)	0.0080	0.0103	0.0117
Debye temperature Θ_D (K)	494.80	573.37	567.62
ρ_1	0.1049	0.1507	0.1620
ρ_2	5.323×10^{-8}	1.162×10^{-6}	1.425×10^{-6}

regime is expressed as $\rho = \rho_0 + \rho_l T^l + \rho_m T^m$, where the first term is the residual resistivity, which includes contributions from temperature-independent disorders like grain boundaries, cationic vacancies, impurity centers, domain wall scatterings, etc. In the second term, the value of l lies between 2 and 3, according to different workers [35–40]. The quadratic dependence with $l = 2$ and $\rho_m = 0$ represents the electron–phonon and electron–electron scatterings. Further, the low temperature phase cannot be considered as an electron system of non-interacting, spin polarized charge carriers. The inclusion of a contribution from spin wave or electron–magnon scattering is better represented by $l = 2.5$ or by the equation $\rho = \rho_0 + \rho_{2.5}T^{2.5}$. A $l = 3$ value is also suggested to include the spin fluctuation scatterings. Alternatively, $l = 2$ and $m = 4.5$ values are reported by Snyder *et al* with the best-fit equation $\rho = \rho_0 + \rho_{2.5}T^{2.5} + \rho_{4.5}T^{4.5}$, which include all the above contributions [40]. The polynomial fits, though, used successfully in the literature suffer from the drawback that the origins behind the individual terms are not very clear. In our samples the residual resistivity ρ_0 increases with increase in x, indicating greater induction of disorders, in agreement with the increase in estimated value of variance, σ^2, with x. Similarly, the effect of lattice distortion and allied phenomena is reflected by the slight rise in the factor ρ_1. The coefficient for the magnetic scattering term ρ_2 increases with higher values of x though the moment per Mn atom, as derived from the neutron diffraction data (described later), remains the same. Since this term is small, a systematic variation could not be found as a function of Hg concentration. However, the sample showed higher values of magnetoresistance in the same order. At low temperatures, the resistivity increases with decrease in temperature due to a Coulomb blockade effect [41].

The electrical behavior of the sample with composition $La_{0.7}Hg_{0.3}MnO_3$ is remarkably different from the other samples. It exhibited not only a higher value of residual resistivity but also a semiconducting behavior followed by a metallic transition at 125 K as shown in figure 4(a). In the high temperature region, a change in slope of the ρ–T curve is seen at $T = 198$ K. A large change in resistivity in the presence of a high magnetic field is seen in the metallic as well as insulating regimes. The magnetic-field-dependent change in resistance is portrayed by the determination of magnetoresistance. The variation of MR values with temperature is shown in figure 4(b). The MR value is maximum (46%) around $T = 198$ K. The MR value is high compared to that of the basic $La_{0.7}Sr_{0.3}MnO_3$ system. In addition, the value is around 35% in the temperature

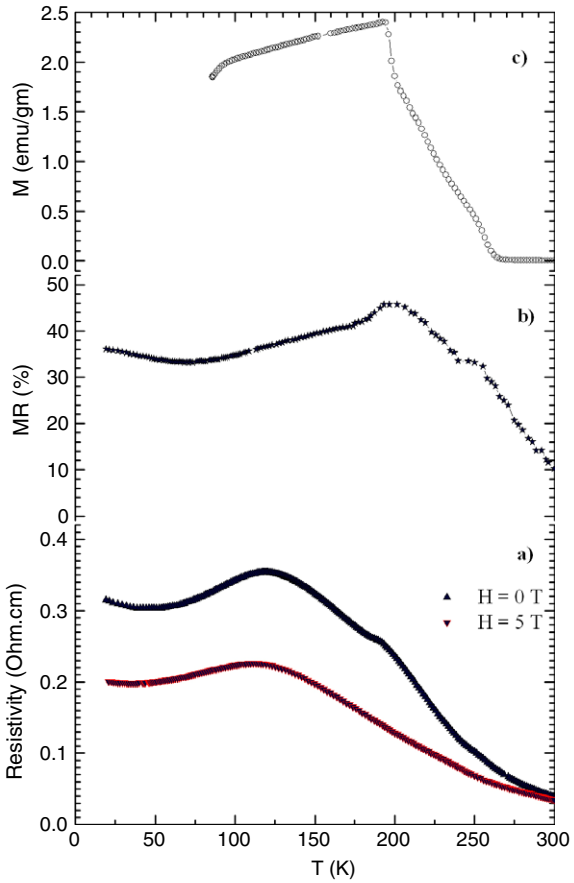

Figure 4. The temperature-dependent electrical and magnetic behavior for the samples with composition $La_{0.7}Hg_{0.3}MnO_3$. (a) Zero field and 5 T magnetic field resistivity; (b) magnetoresistance; (c) zero-field-cooled (ZFC) magnetization with 30 Oe magnetic field. (This figure is in colour only in the electronic version)

range 20 K $\leqslant T \leqslant$ 250 K. Figure 4(c) shows the temperature-dependent variation of zero-field-cooled (ZFC) magnetization. It shows unusual characteristics in terms of a broad paramagnetic to ferromagnetic transition followed by a low temperature cusp. The onset value of the transition temperature ($T_{c\ onset}$) is 260 K and the point of maximum inflection determined from the minimum in the dM/dT curve is 198 K.

In doped manganites the metal–insulator or para-ferro magnetic transition temperatures (T_{MI} or T_C) are primarily determined by the transfer interaction or one-electron bandwidth [3]. The lower value of $\langle r_A \rangle$, and thereby the distortion of MnO_6 octahedra, causes a decrease in these parameters. As a result, reduction in the value of T_{MI} or T_C can occur. For the $x = 0.3$ sample with $\langle r_A \rangle = 1.33$ Å, the expected value of transition temperature is around 270 K [42]. However, there can be large suppression in this value depending on the variance or cationic disorders [6]. Our sample showed a $T_{C\ onset}$ value of 260 K, similar to that reported by Siwach *et al* for the same composition [20]. Nevertheless, in our case the magnetic transition is broad; the T_{MI} value is significantly low and the MR value is high. In this regard, the disorder or the larger value of variance plays a crucial role. Souza and Jardin have reported the broadening of the magnetic transition, which they attributed to the larger distribution of T_C values [43]. The development of nonferromagnetic clusters due to disorders can restrict the FM order to short range. Thus, the weakening of the double exchange interaction operating along the locally distorted Mn–O–Mn path reduces the T_C value and random distribution of FM coupling broadens the width of the transition. Gutierrez *et al* have reported a similar type of behavior and interpreted it in terms of disorder and competing ferromagnetic–antiferromagnetic interaction [44]. Accordingly, nanometer-sized short range ordered FM and AFM regions coexist within grains even above the macroscopic ordering transition temperature. The PM to FM transition is mediated by a spin percolation process. Interestingly, their samples also showed an electrical transition at a temperature significantly lower than those signaling the PM $\rightarrow$ FM transition and a small kink in the resistivity curve is observed at the T_c value. The manganites, particularly with small tolerance factors, are known to show spin glass behavior [45, 46], phase separation [39] and intrinsic inhomogeneities [8]. The observation of a Griffith phase in paramagnetic $La_{1-x}Sr_xMnO_3$ has also been reported [47].

The effect of disorders on electrical behavior is slightly different in the sense that the T_{MI} as well as the width of the resistive transition decreases with increasing disorder [43]. This is associated with the percolative character of the MI transition. The higher degree of disorders in the $x = 0.3$ sample is responsible for the reasonably low value of T_{MI}. The rapid lowering of the T_{MI} may be the combined effect of low Mn–O–Mn bond angle and enhanced atomic disorder. The kink at 198 K may be due to the variation in polaronic character in the range 125 K $\leqslant T \leqslant$ 198 K. Such a change in the nature of hopping, particularly in the lower part of high temperature resistivity, is well known [1, 35]. In the presence of high magnetic field the variation in hopping character of polarons is wiped out and the resistivity follows uniform behavior in the range 125 K $\leqslant T \leqslant$ 300 K. The major ingredients for the polaron formation are the lattice distortion and short range magnetic co-relations [48]. However, it is difficult to resolve the individual contributions merely on the basis of resistivity measurement. Recently Wang *et al* reported that for higher values of σ^2, 'A'-site ions distribute randomly in the lattice without changing microstructure [49]. The disorder can enhance competition between various magnetic and electrical phases, which sometimes results in MR enhancement. We also observed higher MR values than reported [20, 21]. The highest value of MR is obtained at magnetic ordering temperature.

To shed more light on the nature of magnetic ordering, neutron diffraction patterns have been recorded at various temperatures. Neutron diffraction patterns at 17 K for all the samples show enhancement in the intensity of some of the low angle reflections, (012) (110) and (104) in particular, indicating their magnetic origin. The cell parameters contract on lowering of temperature; however no structural transitions were observed. A typical example of a section of the neutron diffraction pattern at 300 and 17 K is shown in figure 5 for an $La_{0.7}Hg_{0.3}MnO_3$ sample. No superlattice reflection was

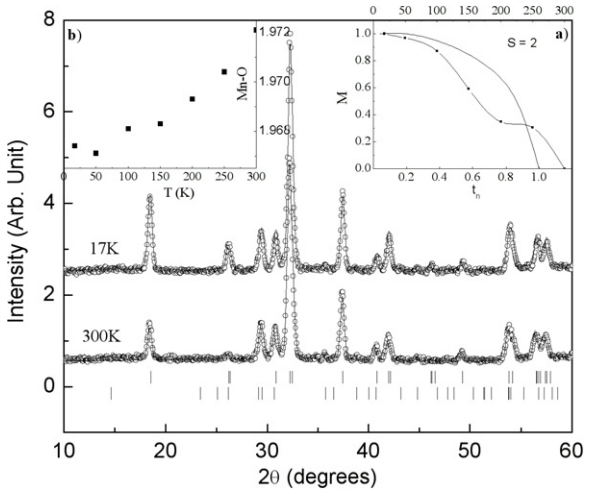

Figure 5. A section of neutron diffraction pattern for the sample with nominal composition $La_{0.7}Hg_{0.3}MnO_3$ recorded at 300 and 17 K. Inset (a) shows variation of magnetic moment obtained from refinement of the powder diffraction patterns recorded at several temperatures, with normalized temperature, ($t_n = T/T_C$). The solid line is the Brillouin function dependence for $S = 2$. Inset (b) shows the variation of the bond length with temperature.

observed indicating the absence of antiferromagnetic ordering. All the samples exhibit long range ferromagnetic ordering. The magnetic moment on the Mn site is obtained from the profile refinement of the diffraction pattern. The magnetic moment at 17 K is found to be $3.5(1)\mu_B$ for all the samples, which is in reasonable agreement with the expected value of moment ($3.7\mu_B$) from a mixture of $Mn^{3+}(4\mu_B)$ and $Mn^{4+}(3\mu_B)$. At 17 K the moment is oriented along the c axis. With increase in temperature an increase in the x component is found, indicating a tilting of the magnetic moment from the c axis. In the inset (a) of figure 5 is shown the variation of magnetic moment as a function of reduced temperature, $t_n(=T/T_C)$. The value of T_C chosen was 260 K as obtained from low field magnetization measurements. The variation of the moment appears to follow the low field magnetization behavior. For comparison, Brillouin function dependence with $S = 2$ is also shown. The deviation from the Brillouin function arises due to the broad paramagnetic to ferromagnetic transition region in this sample, as observed from the low field magnetic measurement. The variation of the bond length with temperature is shown in the inset (b) of figure 5. The bond length varies monotonically with temperature. From this data and analysis we are unable to comment on the nature of the change in distortion, if any, below the metal–insulator transition. The bond angle does not exhibit any variation with temperature and, within error bars, remains at 174.5°. Substitution of Hg for Sr leads to an increase in the variance, σ^2, due to the size mismatch between the two ions. The reduction in T_C is attributed to the increase in σ^2, as reported in other systems [26, 50].

3.3. Microstructural behavior

There is no skepticism regarding the drastic effect of grain boundaries on the charge transport and it has been referred to quite often [32, 35, 51, 52]. The grain boundaries enhance the scattering of conduction electrons due to abrupt changes in periodic potential. They are also the cause of magnetic frustrations as a result of thin (10 Å) and weak coupling between the magnetic domains [32]. Therefore, the decrease in grain size is manifested by a large increase in the residual resistivity [51, 52]. Since our samples have significant

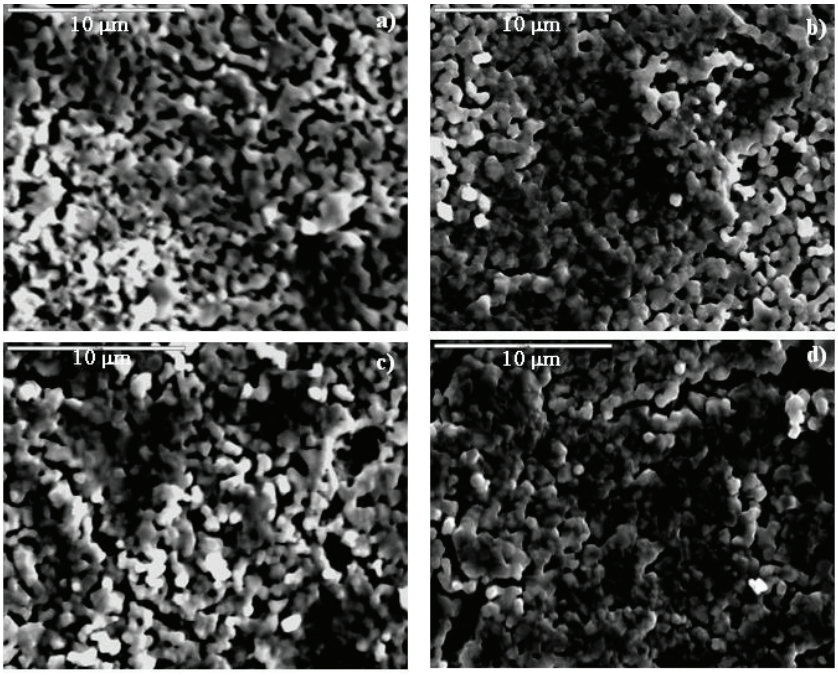

Figure 6. Scanning electron micrographs for the samples with nominal compositions $La_{0.7}Sr_{0.3-x}Hg_xMnO_3$—(a) $x = 0.0$; (b) $x = 0.1$; (c) $x = 0.2$ and (d) $x = 0.3$.

variations in the residual resistivity, it is pertinent to find out the comparative grain boundary contributions. The scanning electron micrographs for all the samples with $x = 0$, 0.1, 0.2 and 0.3 are shown in figure 6. There is no noticeable distinction in the microstructure of these samples. The average grain size of 1–2 μm and uniform grain inter-diffusion is observed in all samples. In fact, the grain morphology is governed mostly by the sample processing methods and the synthesis parameters. The cationic substitution can affect it remotely if the substituent element cements the grain linkage by residing in the grain boundaries or catalyzes the grain growth through partial melting. In the present case, synthesis conditions were identical for all samples. Therefore, microstructural similarity is quite natural. It means the grain boundary contribution to the residual resistivity is the same for all the samples under investigation and the disorders responsible for the observed variations are not, at least on the microscopic scale. This further clarifies that the intrinsic parameters like octahedral distortions and cationic disorders have more influence on the behavior of our samples.

4. Conclusion

We have synthesized polycrystalline samples of an Hg-based CMR system with composition $La_{0.7}Sr_{0.3-x}Hg_xMnO_3$ ($0 \leqslant x \leqslant 0.3$) by the solid state reaction method. For the first time, the neutron diffraction technique was used for the structural analysis of this system. Our study revealed the composition-dependent variation of structural parameters. The calculated values of tolerance factor and average ionic radii showed a decrease with increasing x value whereas the variance increases for the same. The A–O bond length and Mn–O–Mn bond angles show a gradual decrease for higher Hg concentration. The variations in lattice parameters and magnetic moments are also observed. The refined stoichiometry indicates partial substitution of Hg in the base matrix. The samples with $0 \leqslant x \leqslant 0.2$ were metallic below room temperature and the resistivity values could be fitted with an equation containing residual resistivity, Bloch–Gruneisen integral and magnetic scattering terms. The samples with $x = 0.3$ showed a metal–insulator transition at $T = 125$ K with a kink at 198 K. A maximum MR value of 46% and ferromagnetic ordering is observed at this temperature. The microstructures of all the samples were similar, which indicated the intrinsic character of the disorders.

Acknowledgments

The authors are grateful to Dr Rajiv Rawat and Dr Alok Banerjee, UGC-DAE Consortium for Scientific Research, Indore for their cordial help in MR and magnetization measurements. VS is grateful to the M P Council of Science and Technology and University Grants Commission, New Delhi, India for financial assistance.

References

[1] Mott N F 1990 *Metal–Insulator Transitions* (London: Taylor and Francis)
[2] Edwards P P, Johnston R L, Rao C N R, Tunstall D P and Hensel F 1998 *Phil. Trans. R. Soc.* A **356** 5
[3] Imada M, Fujimori A and Tokura Y 1998 *Rev. Mod. Phys.* **70** 1039
[4] Ganguli P 2004 *Curr. Opin. Solid State Mater. Sci.* **8** 385
[5] Rao C N R and Raveau B (ed) 1998 *Colossal Magnetoresistance, Charge Ordering and Related Properties of Manganese Oxides* (Singapore: World Scientific)
[6] Tokura Y 2006 *Rep. Prog. Phys.* **69** 797
[7] Coey J M D, Viret M and Molnar S von 1999 *Adv. Phys.* **48** 167
[8] Loudon J C, Mathur N D and Midgley P A 2002 *Nature* **420** 797
[9] Ahn K H, Lookman T and Bishop A R 2004 *Nature* **428** 401
[10] Haghiri-Gosnet A M and Renard J P 2003 *J. Phys. D: Appl. Phys.* **36** R127
[11] Dorr K 2006 *J. Phys. D: Appl. Phys.* **39** R125
[12] Tao T, Cao Q Q, Gu K M, Xu H Y, Zhang S Y and Du Y W 2000 *Appl. Phys. Lett.* **77** 723
[13] Pi L, Hervieu M, Maignan A, Martin C and Raveau B 2003 *Solid State Commun.* **126** 229
[14] Xu Q Y, Wang R P and Zhang Z 2005 *Phys. Rev.* B **71** 092401
[15] Battabyal M and Dey T K 2006 *J. Phys.: Condens. Matter* **18** 493
[16] Ghatak S K, Kaviraj B and Dey T K 2007 *J. Appl. Phys.* **101** 023910
[17] Xia Z C, Xiao L X, Fang C H, Liu G, Dong B, Liu D W, Chen L, Liu L, Liu S, Doyananda D, Tang C Q and Yuan S L 2006 *J. Magn. Magn. Mater.* **297** 1
[18] Yanga J, Maa Y Q, Songa W H, Zhanga R L, Zhao B C and Sun Y P 2005 *Solid State Commun.* **136** 108
[19] Pena A, Gutierrez J, Barandiaran J M, Chapman J P, Insausti M and Rojo T 2003 *J. Solid State Chem.* **174** 52
[20] Siwach P K, Singh H K, Khare N, Singh A K and Srivastava O N 2003 *J. Alloys Compounds* **350** 56
[21] Shelke V, Khatarkar S, Rawat R and Singh R K 2005 *Solid State Commun.* **135** 208
[22] Rodriguez-Carvajal J 1992 *Physica* B **192** 55
[23] Radaelli P G, Iannone G, Marezio M, Hwang H Y, Cheong S W, Jorgensen J D and Argyriou D N 1997 *Phys. Rev.* B **56** 8265
[24] Shannon R D 1976 *Acta Crystallogr.* A **32** 751
[25] Lufaso M W and Woodward P M 2001 *Acta Crystallogr.* B **57** 725
[26] Rodriguez-Martinez L M and Attfield J P 1996 *Phys. Rev.* B **54** R15622
[27] Dezanneau G, Audier M, Vincent H, Meneghini C and Djurado E 2004 *Phys. Rev.* B **69** 014412
[28] Rodriguez E, Alvarez L, Lopez M L, Veiga M L and Pico C 1999 *J. Solid State Chem.* **148** 479
[29] Mitchell J F, Argyriou D N, Potter C D, Hinks D G, Jorgensen J D and Bader S D 1996 *Phys. Rev.* B **54** 6172
[30] Glazer A M 1975 *Acta Crystallogr.* A **31** 756
[31] Hibble S J, Cooper S P, Hannon A C, Fawcett I D and Greenblatt M 1999 *J. Phys.: Condens. Matter* **11** 9221
[32] Ramakrishnan T V 1998 *Phil. Trans. R. Soc.* A **356** 41
[33] Garcia-Munoz J L, Fontcuberta J, Martinez B, Seffar A, Pinol S and Obradors X 1997 *Phys. Rev.* B **55** R668
[34] Rosenberg H M 1965 *Low Temperature Solid State Physics* (Oxford: Oxford University Press)
[35] Banerjee A, Pal S, Bhattacharya S, Chaudhuri B K and Yang H D 2002 *J. Appl. Phys.* **91** 5125
[36] Urushibara A, Moritomo Y, Arima T, Asamitsu A, Kido G and Tokura Y 1995 *Phys. Rev.* B **51** 14103
[37] Furukawa N 2000 *J. Phys. Soc. Japan* **69** 1954
[38] Ravi S and Kar M 2004 *Physica* B **348** 169
[39] Venkataiah G, Prasad V and Reddy P V 2007 *J. Alloys Compounds* **429** 1
[40] Snyder G J, Hiskes R, DiCarolis S, Beasley M R and Geballe T H 1996 *Phys. Rev.* B **53** 14434

[41] Garcia-Hernandez M, Guinea F, Andres A de, Martinez J L, Prieto C and Vazquez L 2000 *Phys. Rev.* B **61** 9549
[42] Rao C N R, Ramesh R, Raychaudhuri A K and Mahendiran R 1998 *J. Phys. Chem. Solids* **59** 487
[43] Souza J A and Jardim R F 2005 *Phys. Rev.* B **71** 054404
[44] Gutierrez J, Bermejo F J, Barandiaran J M, Cottrell S P, Romano P, Mondelli C, Stewart J R, Barquin L F and Pena A 2006 *Phys. Rev.* B **73** 054433
[45] Chatterjee S and Nigam A K 2002 *Phys. Rev.* B **66** 104403
[46] Dey P, Nath T K and Banerjee A 2007 *J. Phys.: Condens. Matter* **19** 376204
[47] Deisenhofer J, Braak D, Krug von Nidda H A, Hemberger J, Eremina R M, Ivanshin V A, Balbashov A M, Jug G, Loidl A, Kimura T and Tokura Y 2005 *Phys. Rev. Lett.* **95** 257202
[48] Krishnan R V and Banerjee A 2000 *J. Phys.: Condens. Matter* **12** 7887
[49] Wang K F, Yuan F, Dong S, Li D, Zhang Z D, Ren Z F and Liu J M 2006 *Appl. Phys. Lett.* **89** 222505
[50] Rodriguez-Martinez L M and Attfield J P 1998 *Phys. Rev.* B **58** 2426
[51] Gupta A, Gong G Q, Xiao G, Duncombe P R, Lecoeur P, Trouilloud P, Wang Y Y, Dravid V P and Sun J Z 1996 *Phys. Rev.* B **54** R15629
[52] Mahesh R, Mahendran R, Raychaudhuri A K and Rao C N R 1996 *Appl. Phys. Lett.* **68** 2291